R-matrix-incorporating-time method for H_2^+ in short and intense laser fields

Cathal Ó Broin* and L. A. A. Nikolopoulos
School of Physical Sciences, Dublin City University, Collins Avenue, Dublin 9, Ireland
and National Centre for Plasma Science and Technology (NCPST), Collins Avenue, Dublin 9, Ireland
(Received 23 November 2015; published 30 December 2015)

In this work we develop an approach for a molecular hydrogen ion (H_2^+) in the Born-Oppenheimer approximation while exposed to intense short-pulse radiation. Our starting point is the *R*-matrix-incorporating-time formulation for atomic hydrogen [L. A. A. Nikolopoulos *et al.*, Phys. Rev. A **78**, 063420 (2008)], which has proven to be successful at treating multielectron atomic systems efficiently and with a high accuracy [L. R. Moore *et al.*, J. Mod. Opt. **58**, 1132 (2011)]. The present study on H_2^+ is performed with the similar objective of developing an *ab initio* method for solving the time-dependent Schrödinger equation for multielectron diatomic molecules exposed to an external time-dependent potential field. The theoretical formulation is developed in detail for the molecular hydrogen ion where all the multielectron and internuclei complications are absent. As in the atomic case, the configuration space of the electron's coordinates is separated artificially over two regions: the inner (I) and outer (II) regions. In region I the time-dependent wave function is expanded on the eigenstate basis corresponding to the molecule's Hamiltonian augmented by Bloch operators, while in region II a grid representation is used. We demonstrate the independence of our results from the introduced artificial boundary surface by calculating observables that are directly accessed experimentally and also by showing that gauge-dependent quantities are also invariant with the region I box size. We also compare our results with other theoretical works and emphasize cases where basis-set approaches are currently very computationally expensive or intractable in terms of computational resources.

DOI: 10.1103/PhysRevA.92.063428 PACS number(s): 33.80.Rv, 33.80.Gj

I. INTRODUCTION

Currently, a series of rapid developments is impacting strong-field physics because of the discovery and refinement of a diverse range of radiation sources. The construction of free-electron laser sources capable of delivering unprecedented intense radiation in the soft and hard x-ray regimes has initiated new challenges, not only within atomic, molecular, and optical physics but also in a number of other areas at the forefront of current interest more broadly, such as biology, chemistry, and nanoscience. Recently, another advancement, on the opposite end of the wavelength regime, has been the increased availability of intense mid-IR-range radiation [1]. In parallel with the aforementioned recent advances in strong-field physics the production of ultrashort pulses of subfemtosecond duration has allowed the direct experimental observation of electronic and structural dynamics in matter [2].

These technological advances have gained significant attention from the theoretical community, as the simulation of experimental conditions requires significant computational resources which were not previously feasible. For example, for fields into the IR region, as pulse lengths increase and photon energies decrease, the number of angular momenta and the box sizes required for calculating photoelectron spectra increase. Thus, this regime is computationally very demanding and the problem becomes intractable, even for hydrogen (see [3] and [4]) and H_2^+ (see [5]), which are the simplest atomic and molecular systems, respectively.

It is a computationally difficult problem to treat the exact time-dependent response of a multielectron system subject to a strong electromagnetic (EM) field by *ab initio* methods. A number of theoretical groups, worldwide, are aiming for approaches beyond the computationally economical single-active-electron approximation [6–18]; the single-active-electron approach is a mature theoretical method and has been well explored [19,20].

An alternative *ab initio* approach capable of treating multielectron systems is based on *R*-matrix theory applied to atomic and molecular systems for providing structural information [21–23]. The key concept in an *R*-matrix formulation is the *division-of-space* concept, which consists in separating the electrons' configuration space into two regions, namely, the *inner* and the *outer* regions. In the inner region, the atomic-molecular structure of the multielectron states is calculated with all the interactions taken into account, while in the outer region only a single-electron wave function must be calculated [21]. This division-of-space approach appears to be well suited to tackle the computational problem, which becomes especially crucial for the case of a multielectron target. As a matter of fact, the full power of the *R*-matrix formulation is gained in the case of a multielectron target.

Traditionally, *R*-matrix approaches have not considered time dynamics in the study of collision and photoionization processes [24,25]. Within the last decade, in response to technological and experimental advances, variants of time-dependent implementations utilizing the *R*-matrix computational framework have appeared which have been applied to specific atomic systems, namely, the time-dependent *R*-matrix method [26,27], the time-dependent *B*-splines *R*-matrix method [12,28], and the present *R*-matrix-incorporating-time (RMT) method [14,29,30]. An earlier application of the *R*-matrix theory to multiphoton processes appeared in the form of a Floquet expansion of the driven time-dependent wave function [31]. This approach, although it is capable of

*cathal.obroin4@mail.dcu.ie

 ©2015 American Physical Society

treating the field nonperturbatively, cannot be considered to fully follow the time-dependent Schrödinger equation (TDSE) solution methodology since it is only suited to laser pulses containing many cycles.

The formulation of the time-dependent R-matrix method was developed and first applied to a one-dimensional model by Burke and Burke [26] and later generalized and successfully applied to neon and argon [32,33]. The time-dependent R-matrix method generates the R-matrix eigenstates in the inner region using an extension of the R-matrix Belfast codes [34] to include a B-splines expansion of the continuum spectrum. Then the system's time-dependent wave function is propagated using a second-order Cayley propagator, while in the outer region the time-dependent propagation is based on an R-matrix propagator, employed for solving a system of coupled second-order differential equations [22].

In the time-dependent B-splines R-matrix method, the R-matrix eigenstates are generated using an alternative implementation of R-matrix theory on a nonorthogonal basis approach (B splines) [35] and are propagated with an Arnoldi-Lanczos algorithm [36]. However, the current implementation of the time-dependent B-splines R-matrix method performs the wave-function propagation only in an (enlarged) inner region, ignoring the outer region completely, and as such does not fully take advantage of the division-of-space formulation of the R-matrix method. Nevertheless, the obtained results are also indicative of the powerful machinery of the R-matrix methods at describing multiphoton processes in complex systems.

The RMT method for atomic systems was mainly developed for the possibility of combining a high-order time propagator for the multielectron wave function expanded on the inner-region R-matrix eigenstates with a finite-difference method for the grid representation of the single-electron wave function in the outer region. The method was first formulated and applied to the ionization of hydrogen [29] and later extended to include the single ionization of multielectron systems [14,30]. This *unique* combination of an eigenstate-basis method with the finite-differences technique of propagating the time-dependent wave function was recently shown by Wragg *et al.* [37] to demonstrate the capability of describing double-electron outer-region wave functions.

The RMT method not only allows the possibility of reducing the multielectron dimensionality of the initial formulation to, effectively, a one (or two)-electron calculation in the (radially) larger region II, but also allows the use of different algorithmic approaches in the two regions (Fig. 1). In region I the power of the R-matrix method to calculate very accurate energy eigenfunctions and transition matrix elements is fully exploited, while in the outer region the extensibility of an equidistant, grid-based, representation of the wave function to very large distances dramatically enhances the computational performance.

In contrast with the above activities focused on atomic systems, analogous time-dependent formulations based on the division-of-space concept for molecular systems are not common. These methods include the t-surff method developed by the group of Scrinzi [38,39] and the analytical R-matrix method developed and applied in multielectron molecular systems [40–42]. Despite the fact that a number of groups worldwide have developed unique expertise in developing

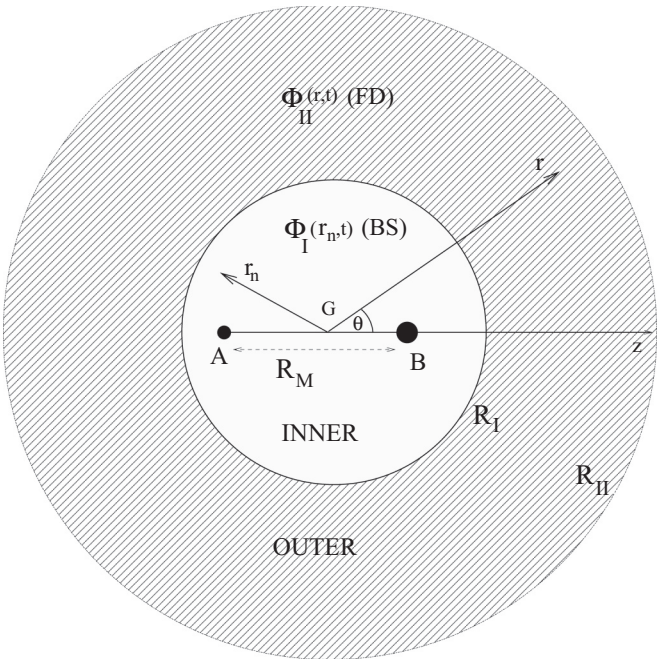

FIG. 1. Sketch of the division-of-space method in the general diatomic situation (see [29] for a similar hydrogen diagram). The two nuclei are labeled A and B and the internuclear distance is R_M. By $\mathbf{r}_n, 0 \leqslant r_n \leqslant R_{\rm I}$ we denote collectively the positions of all electrons relative to a coordinate system with its origin placed at the molecule's center of mass, G, and the z axis along the internuclear axis. With $\mathbf{r} \equiv (r,\theta,\phi)$, $R_{\rm I} \leqslant r \leqslant R_{\rm II}$ we represent the position of the ejected electron following the molecule's excitation-ionization by the external radiation. The molecule's configuration space is divided into two homocentric spherical boxes, (inner region, I, and outer region, II, with radii $R_{\rm I}$ and $R_{\rm II}$, respectively), with their center place at G. The molecule's time-dependent wave function in the inner region, I, is expanded on an eigenstate basis (BS) $\Phi_I(\mathbf{r}_n,t)$. In the outer region, II, the system's wave function is described only by the ejected electron's wave function $\Phi(\mathbf{r},t)$ using a finite-difference (FD) approach. In the present case of a one-electron system, $\mathbf{r}_n \equiv \mathbf{r}$.

sophisticated *ab initio* methods and applied them to solve the TDSE for molecules, it appears that these groups have not investigated the R-matrix method in this context.

In this work we introduce an approach based on an extension of the RMT method to H_2^+ without the complications arising from multielectron considerations. Since the hydrogen molecule ion is also of interest for the RMT approach as a stepping stone towards a full treatment of the hydrogen molecule and on to other polyatomic systems, we develop the method in detail and demonstrate its applicability to diatomic one-electron systems with the EM field aligned along its symmetry axis in the fixed-nuclei approximation.

In addition to the above scope, the present work also aims to ensure efficiency in the *ab initio* description of molecules in intense and short EM fields. To this end, we have developed the formulation for (and implemented) the velocity-gauge interaction operators in addition to the length-gauge alternative. As is generally known, for these studies, the velocity gauge is preferred against the length gauge for radiation in the long-wavelength regime because of its better convergence properties [43]. It is worth emphasizing that this

publication demonstrates the first usage of this gauge within the time-dependent *R*-matrix approaches discussed above and in the existing RMT codes. Moreover, the RMT computations are done through General Purpose Computation on Graphical Processing Unit techniques similar to our earlier works, albeit with some extra complexity [44,45].

The paper is organized as follows. In Sec. II we give an overview of the basic theory. This is the key section of this paper, where we set out in detail the theoretical formulation for the case of one-electron homonuclear diatomic molecules. The formulation presented in this section can be generalized to include the case of one-electron nonhomonuclear diatomic systems with little extra effort. We also give the expressions for the calculation of experimental observables adapted to our methodology. In Sec. III to ensure the validity of the method, experimentally accessible quantities are compared to similar theoretical calculations available from the literature. Finally, we have relegated the main technical details to the appendixes. In the presentation of the formulas, atomic units are used ($m = \hbar = |e| = 1$) throughout.

II. THEORETICAL FORMULATION

For the current case of short but intense fields, the Born-Oppenheimer approximation [46] is assumed so that the nuclei are effectively static over the short duration of the pulse. We also assume that the radiation field is linearly polarized along the symmetry axis of the diatomic molecule. Without loss of generality, we take the molecular axis as the z axis of an $Oxyz$ Cartesian coordinate system. In this fixed-nuclei approximation the electronic Hamiltonian of the molecular hydrogen ion is given by

$$H_0 = -\frac{\nabla^2}{2} - \frac{Z}{|\mathbf{r} - \mathbf{R}_M/2|} - \frac{Z}{|\mathbf{r} + \mathbf{R}_M/2|},$$

where Z is the atomic number and $\pm\mathbf{R}_M/2$ the position of the nuclei in the chosen coordinate system. Since the internuclear distance, $R_M = |\mathbf{R}_M|$, is treated as a constant term in the Hamiltonian, the $1/R_M$ term is omitted since it does not impact the electron dynamics.

The rotational properties of this one-electron diatomic system are more complex than in the atomic single-electron case, thus making the problem considerably more demanding, both conceptually and computationally. Rotational symmetry is broken in H_2^+ since rotation of the system along the x and y axes is not equivalent to rotation along the z axis. This means that the orbital angular momentum operator $\mathbf{L}^2$ fails to commute with the Hamiltonian, as $\mathbf{L}^2$ is the generator of rotation, while the L_z operator will still commute (z-axis projection). Thus the Hamiltonian and the orbital angular momentum operators do not have shared eigenfunctions. As a result, the time-dependent wave function of the system is not expanded in terms of a linear combination of mutual eigenfunctions of H and L_z and the parity operator Π with associated eigenvalues ϵ, μ, and λ, respectively. The parity can be gerade (even; $\lambda = 0$) or ungerade (odd; $\lambda = 1$), reflecting whether or not the state is symmetric or antisymmetric through a mirror reflection on the x,y surface along the z axis. In the particular case of study, the interaction of H_2^+ with a linearly polarized field along the molecular axis, it is routinely shown that the excited states should have the same μ symmetry number as the initial state ($\mu = 0$). This allows us to neglect the μ quantum number, since the initial state in the present case is the H_2^+ ground state $1\sigma_g$.

The propagation of the electron wave function for a system of H_2^+ in the presence of an external laser field is calculated through the solution of the corresponding TDSE:

$$i\frac{\partial}{\partial t}\Phi(\mathbf{r},t) = [H_0 + D(\mathbf{r},t)]\Phi(\mathbf{r},t).$$

The expression for the basis expansion in terms of the energy eigenfunctions of H_0 is

$$\Phi(\mathbf{r},t) = \sum_{n\lambda} C_{n\lambda}(t)\Phi_{n\lambda}(\mathbf{r}), \tag{1}$$

where $\Phi_{n\lambda}$ are solutions of the field-free Hamiltonian (see Appendix A for details) and the index n is associated with the system's eigenenergies ($\epsilon_n \leftrightarrow n$) and denotes both bound and (discretized) continuum eigenstates. Equivalently, the wave function can also be represented as a partial-wave expansion,

$$\Phi(\mathbf{r},t) = \sum_{l} \frac{1}{r} f_l(r,t)Y_{l0}(\Omega), \tag{2}$$

where the eigenvalues of the angular momentum operator $\mathbf{L}^2$ are characterized by the index l. At this stage, further description of the calculational method requires the separate treatment of the TDSE for the inner and the outer regions.

A. The TDSE in the inner region

For the basis approach in region I the time-independent Schrödinger equation (TISE) associated with H_0 would be non-Hermitian if there was a naive division of the full space. To cope with the non-Hermiticity of the operators appearing in the TISE the same approach as in the case of atomic hydrogen [29] is followed. First, the field-free Hamiltonian and the velocity gauge dipole-interaction operator are augmented to become their Hermitian counterparts within the spherical region $[0, R_I]$,

$$\hat{H}_0(\mathbf{r}) = H_0(\mathbf{r}) + \hat{L}_h(\mathbf{r}), \tag{3}$$

$$\hat{D}(\mathbf{r},t) = D(\mathbf{r},t) + \hat{L}_d(\mathbf{r},t), \tag{4}$$

where $\hat{L}_h$ and $\hat{L}_d$ are the corresponding Bloch operators (see Appendix B). Then the augmented TISE is diagonalized.

So for region I, the eigenfunction expansion in Eq. (1) is modified to

$$\Phi_I(\mathbf{r},t) = \sum_{n\lambda} \tilde{C}_{n\lambda}(t)\tilde{\Phi}_{n\lambda}(\mathbf{r}), \tag{5}$$

where $\tilde{\Phi}_{n\lambda}(\mathbf{r})$ are now energy eigenfunctions of the *Bloch-augmented* Hamiltonian and $\tilde{C}_{n\lambda}(t)$ is the associated time-dependent coefficient.

Equating the expressions for the time-dependent wave function Eqs. (1) and (2), whilst decomposing the energy eigenfunctions in terms of spherical harmonics, we have

$$\sum_{n\lambda} \tilde{C}_{n\lambda}(t) \sum_{l\in l_\lambda} \frac{1}{r} P_{nl}(r)Y_{l0}(\theta) = \sum_{\lambda, l\in l_\lambda} \frac{1}{r} f_l(r,t)Y_{l0}(\theta), \tag{6}$$

and after some straightforward manipulations we arrive at the following time-dependent partial-wave relation in terms of the radial eigenstates P_{nl_λ} for the inner region:

$$f_{l_\lambda}(r,t) = \sum_n \tilde{C}_{n\lambda}(t) P_{nl_\lambda}(r), \quad r \leqslant R_{\rm I}. \tag{7}$$

Clearly, this expansion only holds in the interval $(0 < r \leqslant R_{\rm I})$ since the Bloch eigenfunctions are not defined outside this region.

Finally, the initial TDSE is maintained by subtracting both of the Bloch operators from the TDSE. So the TDSE expressed in terms of these Hermitian operators is

$$i\frac{d}{dt}\Phi_{\rm I}(\mathbf{r},t) = [\hat{H}_0(\mathbf{r}) + \hat{D}(\mathbf{r},t) + S(\mathbf{R}_{\rm I},t)]\Phi_{\rm I}(\mathbf{r},t), \tag{8}$$

where $S(\mathbf{R}_{\rm I},t) = -\hat{L}_h(R_{\rm I}) - \hat{L}_d(\mathbf{R}_{\rm I},t)$. More specifically, in the current implementation, with the use of Eqs. (B3) and (B6) the boundary term in the velocity gauge is

$$S(\mathbf{R}_{\rm I},t) = -\frac{1}{2}\delta(r-R_{\rm I})\left[\frac{d}{dr} + \frac{1}{r} - i\frac{A(t)}{c}\cos\theta\right].$$

This equation is fully equivalent to the initial TDSE without any approximation involved. It is also worth emphasizing that the extra terms which are added and subtracted away are *only nonzero on the boundary surface* $r = R_{\rm I}$. The $\frac{d}{dr}$ and $\frac{1}{r}$ terms on the right-hand side are due to the operator $\hat{L}_h$, while the last term is due to the interaction operator $\hat{L}_d$. The corresponding expression for the boundary term in the case of the length-gauge formulation is the same except that this latter term is not present.

In region I the eigenfunctions and eigenvalues of the Hermitian Hamiltonian $\hat{H}_0$ should now be calculated. Then the functions $\tilde{\Phi}_{n\lambda}(\mathbf{r})$ from Eq. (5) can be used to represent the inner-region portion of the TDSE as a system of first-order ordinary differential equations. This will allow the calculation of the time-dependent coefficients, $\tilde{C}_{n\lambda}(t)$, at some time t from a known initial state.

At this point we relegate the detailed development of the relevant formulation [namely, the calculational procedure for the field-free problem $\hat{H}_0\Phi_{n\lambda}(r) = \epsilon_{n\lambda}\Phi_{n\lambda}(\mathbf{r})$] to Appendixes A and B. Assuming that the field-free problem is solved, the wave function is expanded on these specific eigenfunctions of the field-free Bloch-augmented Hamiltonian, to arrive at

$$i\frac{d}{dt}\tilde{C}_{n\lambda}(t) = \sum_{n'\lambda'}[\hat{H}_{n\lambda,n'\lambda'} + \hat{D}_{n\lambda,n'\lambda'}(t)]\tilde{C}_{n'\lambda'}(t) + \int d^3r\,\Phi_{n\lambda}(\mathbf{r})S(\mathbf{R}_{\rm I},t)\Phi_{\rm II}(\mathbf{r},t), \tag{9}$$

where $\hat{H}_{n\lambda,n'\lambda'}$, $\hat{D}_{n\lambda,n'\lambda'}(t)$ are the matrix elements of the operators $\hat{H}_0(\mathbf{r})$, $\hat{D}(\mathbf{r},t)$, respectively. The time-dependent wave function $\Phi_{\rm II}(\mathbf{r},t)$ is labeled II since we use the grid expansion, (2). This expansion is also the one that is used in region II. Therefore, in the last term we do not use terms solely of the inner-region basis but rather $\Phi_{\rm II}(\mathbf{R}_{\rm I},t)$, since the $\delta(r-R_{\rm I})$ function in the boundary operator $S(t)$ contains derivatives. Calculation of the derivative of $\Phi_{\rm II}(\mathbf{R}_I,t)$ requires information from both region I and region II. The expansion of the inner-region radial functions in terms of the partial waves through Eq. (7) at specific (inner-region) points allows the finite-difference spatial operators to be calculated by using the required values.

The reduction of the matrix element between a Bloch-energy eigenstate and an angular momentum eigenstate implied by the coupling term of Eq. (9) (final term on the right-hand side) is effectively the same as in the hydrogenic case [29], except there is a summation over the partial-wave terms within the same symmetry. Summarizing all the above reductions we obtain the TDSE in the inner region and in the velocity gauge as

$$i\frac{d}{dt}\tilde{C}_{n\lambda}(t) = \epsilon_{n\lambda}\tilde{C}_{n\lambda}(t) + \sum_{n'\lambda'\neq\lambda}\tilde{C}_{n'\lambda'}(t)D_{n\lambda,n'\lambda'}(t) - \frac{1}{2}\sum_{l\in l_\lambda}P_{nl}(R_{\rm I})F_l(R_{\rm I},t), \tag{10a}$$

$$F_l(R_I,t) = \frac{d}{dr}f_l(R_{\rm I},t) - i\frac{A(t)}{c}\sum_{l'=l\pm1}K_{ll'}f_{l'}(R_{\rm I},t). \tag{10b}$$

In the length gauge the inner-region TDSE is obtained if we set $A(t) = 0$ in the above expression for the $F_l(R_{\rm I},t)$ term. The quantity $K_{ll'}$, as given in Appendix A, originates from the angular momentum properties of the dipole interaction term. Formally, the above inner-region TDSE differs from the corresponding one of the atomic case in that the appropriate quantum number to characterize stationary states changes from l to λ, while the boundary surface term includes a summation over all the coupled (due to the molecular potential) orbital angular momenta l, belonging to the same symmetry λ.

B. The TDSE in the outer region

The molecular hydrogen ion grid form is derived in a standard way. The final equation in terms of a radial grid is

$$i\frac{\partial}{\partial t}f_l(r,t) = \left[-\frac{1}{2}\frac{\partial^2}{\partial r^2} + \frac{l(l+1)}{2r^2}\right]f_l(r,t) + \sum_{l'\in l_\lambda}V_{l0,l'0}(r)f_{l'}(r,t) + \sum_{l'\notin l_\lambda}D_{l0,l'0}(r,t)f_{l'}(r,t),$$

$$V_{l0,l'0}(r) = -2Z\delta_{(l+l')\,\rm even}\sqrt{(2l+1)(2l'+1)} \times \sum_{L=|l-l'|,|l-l'|+2,\ldots}^{l+l'}\frac{r_<^L}{r_>^{L+1}}\begin{pmatrix} l & L & l' \\ 0 & 0 & 0\end{pmatrix}^2, \tag{11}$$

where $r_> = \max(r, R_M/2)$, $r_< = \min(r, R_M/2)$, and $D_{l0,l'0}(r,t) = \langle l0|D(\mathbf{r},t)|l'0\rangle$. The difference for the RMT case is that the grid is not calculated over the full space but is limited to region II. The derivative for the point $r = R_{\rm I}$ is calculated by using Eq. (7) to calculate the partial-wave grid points from within region I as required. More details are given in Appendix C.

At large distances from the molecular center, relative to the separation of the nuclei ($r \gg R_M$), the dominant part of the molecular potential is the spherically symmetric part, making it effectively hydrogenic. So, the potential term can be switched to that of a hydrogenic system to a very good approximation. In a regular basis calculation this would not help to make

the calculation more manageable in terms of size during the propagation because the symmetry of the system close to the nuclear center dictates the properties of the eigenfunctions.

C. Bound-state populations and ionization yield

In the RMT approach information from regions I and II is required to calculate observables and other quantities. In region I, the information must be extracted from the energy eigenfunctions $\tilde{\Phi}_{n\lambda}(\mathbf{r})$ and the associated coefficients $\tilde{C}_{n\lambda}(t)$. For region II, the partial waves $f_{lm}(r,t)$ and the spherical harmonics are available.

The most straightforward quantities to calculate for the basis, finite-difference, and RMT methods, for comparison, are the ground-state population, the excited-state population, and the total ionization yield. The ground-state population $p_g(t)$ is calculated by the overlap of the initial state $\Phi(\mathbf{r},0)$ onto the state at time t, $\Phi(\mathbf{r},t)$. If the ground state of the system is initially populated, the evolution of the ground-state population is

$$p_g(t) = \left| \int d^3r \, \Phi^\star(\mathbf{r},0)\Phi(\mathbf{r},t) \right|^2. \tag{12}$$

Within the RMT method the above integral is broken up into two separate integrals, one from 0 to R_I and another from R_I to the outer boundary R_II,

$$p_g(t) = \left| \int_0^{R_\mathrm{I}} dr r^2 \int d\Omega \, \Phi^\star(\mathbf{r},0)\Phi(\mathbf{r},t) + \int_{R_\mathrm{I}}^{R_\mathrm{II}} dr r^2 \int d\Omega \, \Phi^\star(\mathbf{r},0)\Phi(\mathbf{r},t) \right|^2, \tag{13}$$

which is the statement that the ground-state population has contributions from both regions $p_g(t) = |p_{g;\mathrm{I}}(t) + p_{g;\mathrm{II}}(t)|^2$, where $p_{g;\mathrm{I}}(t)$ and $p_{g;\mathrm{II}}(t)$ are the contributions from the respective regions. For the region I portion, the calculation is simply the sum

$$p_{g;\mathrm{I}}(t) = \sum_{n\lambda} \tilde{C}^\star_{n\lambda}(0)\tilde{C}_{n\lambda}(t). \tag{14}$$

In a basis calculation, the coefficient corresponding to $1\sigma_g$, $C_{10}(0)$, equals 1 and the ground-state population calculation is provided by the square of the corresponding time-dependent coefficient $|C_{10}(t)|^2$, after the end of the pulse. Similarly, the absolute value of the coefficient $|C_{n\lambda}(t)|^2$, postpulse, gives the population of the $|n\lambda\rangle$ eigenstate. In the RMT method the absolute value of $|\tilde{C}_{n\lambda}(t)|^2$ does not have the same relationship with the surviving populations of $H_2{}^+$. This is because, in region I, the physical bound states are composed by a linear combination of all of the (normalized) RMT eigenfunctions within the symmetry. For this reason the ground-state population requires the full calculation of the sum in Eq. (14) rather than only the first term as in the basis method. For the finite-difference region, region II, an explicit spatial overlap must be calculated (approximately through the composite Simpson's rule) through direct integration:

$$p_{g;\mathrm{II}}(t) = \sum_l \int_{R_\mathrm{I}}^{R_\mathrm{II}} dr f^\star_{l0}(r,0) f_{l0}(r,t). \tag{15}$$

As a result, the total ground-state population is

$$p_g(t) = \left| \sum_{n\lambda} \tilde{C}^\star_{n\lambda}(0)\tilde{C}_{n\lambda}(t) + \sum_l \int_{R_\mathrm{I}}^{R_\mathrm{II}} dr f^\star_{l0}(r,0) f_{l0}(r,t) \right|^2.$$

While the bound and ionized populations can also be trivially calculated by an appropriate summation in the basis case, for the RMT case this information is lost (due to the mixing of *R*-matrix states). Since the partial waves can be reconstructed, the approach for the finite-difference case can also be used. For the finite-difference case, the population of the bound states can be approximated by direct spatial integration of the probability values at all grid points inside a carefully chosen radius, say r_i,

$$p_b(t) = \sum_l \int_0^{r_i} dr \, |f_{l0}(r,t)|^2, \tag{16}$$

where care is taken in choosing r_i such that the population of the bound state is converged with increasing radius.

Considering that the system only consists of bound and ionized states, knowing the bound-state population means that the ionized population is also known $[1 - p_b(t)]$. In the RMT case, the exact equivalent of this bound-population calculation can be done by simply getting the population of region I through the coefficients, $\tilde{C}_{n\lambda}(t)$ (if R_I is selected as the ionization boundary):

$$p_b(t) = \sum_{n\lambda} |\tilde{C}_{n\lambda}(t)|^2. \tag{17}$$

This also ensures that no numerical integration is required. Otherwise, the same numerical integral as in the ground-state case can be used. It should be emphasized that the methods of calculating the ionization yield in the finite-difference and RMT methods both require postpulse propagation. This means that the ionized population cannot be easily distinguished from the bound-state population during the run of the pulse. The excited-state population, for example, is approximated by the quantity within a subset of the total box which is not counted towards ionization and which is not the ground state $[p_b(t) - p_g(t)]$. Note that it is not until the postpropagation, when the ionized population moves away from the central potential and the yield value asymptotically approaches a value, that the excited-state population becomes meaningful.

To ensure that a reasonable part of the contributions from continuum energy-eigenstates are counted in the ionization yield postcalculation, the wave equation is propagated forward in time. This allows the continuum contributions to move away from the central boundary so that the yield can be calculated by counting the probabilities after a certain cutoff radius (R_I is ideal for the RMT case). The radius should be chosen so that a minimal amount of bound-state probability is included in the ionization yield calculation.

III. RESULTS AND DISCUSSION

Prior to discussing particular applications it is worth discussing computational issues at a more general level. The eigenstate-basis method for the solution of the TDSE requires the precomputation of the associated field-free Hamiltonian eigenproblem (say, of size n_max) for partial waves up to

$l_{\max} - 1$. The latter numbers are dictated mainly by the strength and the duration of the EM field. Intense fields induce multiphoton absorptions that result in populating states with higher energy and orbital angular momentum quantum numbers.

For a reasonable energy spacing including higher energies ranges and to ensure that the box is sufficiently large to capture the dynamics, a larger box size with a spatial discretization which is sufficiently dense enough to represent the highest energies is required. Both effects increase the size of the eigenproblem. For example, if the knot point spacing in the basis grid is taken to be approximately equidistant over the full box size, then the computational effort for the number of eigenvalues and eigenvectors, $n_{\max}$, to be found from the diagonalization will scale linearly with both the box radius and $l_{\max}$. Further, the corresponding transition matrix element block scales with the square of both the box radius and $l_{\max}$. Approximately commensurate with the increase in the number of states per partial wave, the number of partial waves included must also be increased to account for the greater occupancy of partial waves which have a higher angular momentum number. This results in a rough scaling law for the total number of the states to be included of $\sim(n_{\max} l_{\max}/2)$, while the number of transition matrix elements required for computation will be $\sim n_{\max}^2 l_{\max}^2/4$. In practice, both of these numbers are determined by testing the convergence of the specific value or set of values under study, such as the expectation value, etc., against a gradual increase in the available parameters. Consequently, the total impact of increasing the size of these parameters is to make the field-free precomputation as well as the propagation of a basis calculation prohibitively expensive. It leads to the highly undesirable condition of a Hamiltonian which should be approximated in a large spatial region with a very fine grid and a large number of coupled angular momentum terms. It is for the above reasons that we have relied on the present extension RMT method combined with a parallel implementation for diatomic systems. The RMT approach only requires a basis representation in a restricted region of space, which thus restricts the computational burden significantly. Whatever computational hurdle remains is then tackled with a parallel treatment. We now turn to the calculation of population and ionization yields of H_2^+ for specific cases.

A. Calculation of the initial state of H_2^+ by propagating the diffusion equation

The calculation of the initial state proceeds by propagation of the resulting (diffusion) equations in the inner and outer regions after setting the external EM field equal to 0 and by removal of the complex number from the TDSE. Formally, the associated diffusion equation is obtained by making the substitution $t \to \imath t$ in the original field-free TDSE. In our calculation we set $l_{\max} = 24$. We compare our RMT calculations for the ground state of H_2^+ using a purely basis method (BS) [44] and a purely finite-difference method after having extended the finite-difference code in Ref. [45] to include the H_2^+ system. As previously reported by Martin [48], 20 angular momentum terms provides a very decent estimate of the H_2^+ ground-state energy ($-1.102\,50$ a.u., compared to an exact value of $1.102\,63$ a.u). This means that the 24 partial waves we have used should provide a reasonable measure. The calculated energy is $E_g^{\mathrm{FD}} = -1.0942$ a.u in the purely finite-difference method, an error of about 0.765%. In the present RMT calculation, which consists of a mixed basis-finite difference propagation of the diffusion equation, the energy found is $E_g^{\mathrm{RMT}} = -1.102\,532$ a.u. This is very close to that achieved by Martín [48] ($1.102\,50$ a.u. for 20 $l_{\max}$). We have also calculated the ground-state eigenenergy with a purely eigenstate basis and found $E_g^{\mathrm{BS}} = -1.102\,532$. The outer-region box radius was $R_{\mathrm{II}} = 713.1$ a.u. for the RMT and the finite-difference method. For the BS method $R_{\mathrm{II}} = 99.9$ a.u. For the RMT and the BS method the B splines were of order $k = 10$. In the RMT method the boundary radius was $R_{\mathrm{I}} = 12.9$ a.u. The chosen grid spacing in the outer region was $dr = 0.2$ a.u. In the inner region, the chosen knot sequence $t = (t_1, t_2, \ldots, t_{n_b})$ of the B-splines grid was $t = P(0.0, 0.125, 0.25, 0.375, 0.5, 0.625, 0.750, 0.875, 0.95, 1.00, 1.05, 1.125, 1.25, 1.5, 1.7, 1.9, \ldots$ (increments of 0.2) $\ldots 12.9)$ a.u.

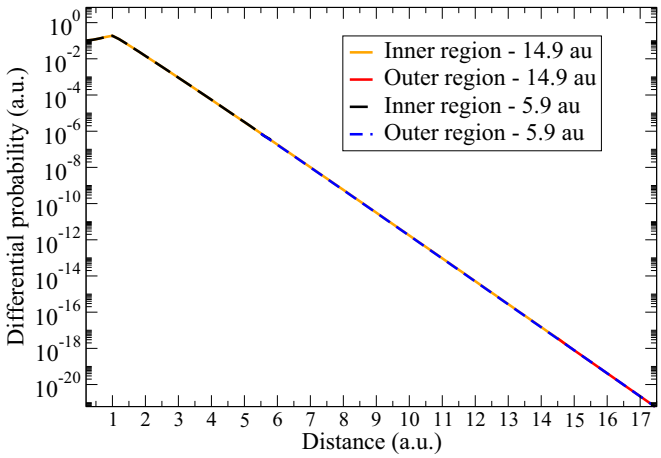

FIG. 2. (Color online) A comparison of two H_2^+ R-Matrix incorporating Time (RMT) diffusion calculations, with two inner-outer region divisions, 5.9 and 14.9 a.u. There are no major discrepancies between the different box sizes. The wave function calculated along z is shown.

In Fig. 2 we show the wave functions evaluated along the z axis with two inner- and outer-region boundary sizes, at $R_{\mathrm{I}} = 5.9$ a.u. and $R_{\mathrm{I}} = 12.9$ a.u. We see that the H_2^+ results are consistent regardless of box size. Note that a finer grid spacing along the boundary is required in the present RMT approach than would strictly be required in a standard basis calculation of the same size, since now the actual radial representation is important, and not just the dipole and energy values.

B. Populations and ionization yields H_2^+ under EM fields

Being confident in the calculation of our ground state through the RMT diffusion propagation method, we now look at the time evolution of the wave function in an external EM field. First, we consider the case of making sure the dynamics follows what we would expect in terms of multiphoton absorption. We take a pulse that is so short that most of the ionization takes place at the peak of the pulse. If the initial wave function is treated as though it were initially localized in a small region close to $r = 0$, which is indeed the case for the ground state, we then propagate the system

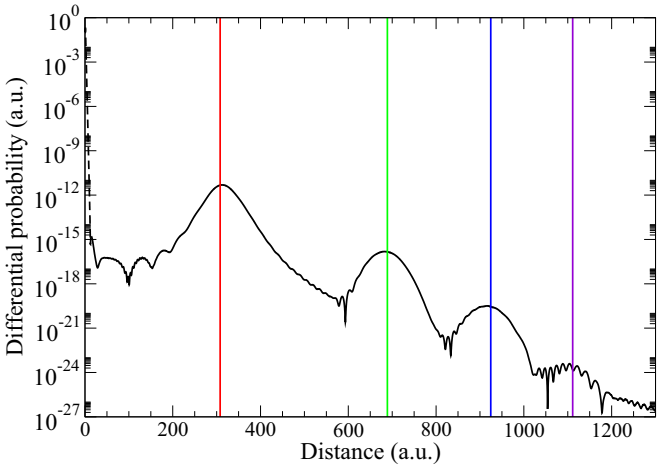

FIG. 3. (Color online) Projection of the wave function along z after a 24-cycle laser pulse and postpropagation three times the length of the pulse is shown. The inner-region portion of the wave function is shown as the dotted black line; the outer region, as the solid black line. The expected positions of the different wave-packet peaks are also shown (from left to right): one-photon (red vertical line), two-photon (green vertical line), three-photon (blue vertical line), and four-photon (violet vertical line) absorption electron wave packets.

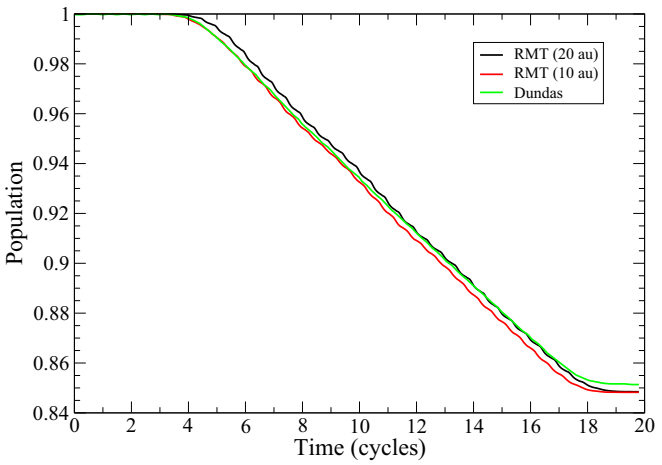

FIG. 4. (Color online) The bound-state population compared with digitized data from Dundas *et al.* [47]. The pulse is trapezoidal, with a central photon energy of 5.4523 eV, with a 4-cycle cosine ramp, a 12-cycle main portion, and a 4-cycle cosine ramp down. The intensity is 4×10^{14} W cm^{-2}.

such that the ionized portions of the wave function travel distances several times longer than the length of the molecule. We use a sine-squared pulse of carrier frequency $\omega = 40$ eV so that any photon absorptions bring the $H_2{}^+$ straight into the continuum at a velocity corresponding to 10 eV for the case of one-photon absorption. The different wave packets corresponding to the different numbers of absorbed photons (above-threshold ionization peaks) should spatially separate out, as they correspond to different acquired velocities. The formula for the distance away from the molecule is then quite simple: $r_n \sim (t - t_i)\sqrt{2E_n}$ a.u., with $n = 1,2\ldots$.

In Fig. 3 we plot a snapshot of the radial wave function. The wave-packet peaks are clearly separated and align with the expected distance considering the photon absorption count and the total ionized propagation time, which is $3.5\tau_p$ if the total duration of the calculation is $t = 4\tau_p$ (since the travel time of the wave packet is after the time that the ionization takes place, which we take to be at the pulse's peak time at $t_i \sim 0.5\tau_p$).

In Fig. 4, we show the results of Dundas *et al.* [47] versus the current RMT calculation. In the figures we show the results by assuming two boundaries for the ionization thresholds for calculation of the bound-state population; $R_I = 10$ a.u and $R_I = 20$ a.u. In calculating the bound-state population we assume the norm of the time-dependent wave function at distances $r < R_I$. The final ionization yield for Dundas *et al.* is 0.851 (Dundas) and 0.848 (10 and 20 a.u, respectively), a disagreement of 0.353%. Within the present RMT approach the bound states are well represented, as the knot density can be increased close to the atomic nuclei without having a major impact on the overall number of splines.

Next, in Table I we compare our ionization yields obtained with the pure basis (BS) and RMT methods with the results obtained by Guan *et al.* [13]. The RMT yields are calculated by treating the inner-region population as the bound-state population after one additional laser pulse length of field-free propagation. The bases are heavily modified in the inner region and have a continuum spacing down to 0.4 a.u up to a radial distance of 138 a.u., while $l_{max} = 15$. The velocity gauge was used in all calculations. The pulse used has a sine-squared envelope with a photon energy of $\omega = 40$ eV and its duration was 10 cycles in total. Our results are in agreement with those of Guan *et al.* within 0.5% except for the highest intensity, which disagrees by 2%. This represents a good agreement, particularly considering the very different methods used; Guan *et al.* use a finite-element DVR technique and prolate spheroidal coordinates. Comparing the basis and RMT methods themselves, the results are effectively identical. As a last comment on these results, note that the calculated ionization yields have a linear dependence on the pulse's peak intensity $Y \sim I_0$, consistent with the fact that the ionization is possible by a single-photon absorption since $\omega = 40$ eV.

C. Length- and velocity-gauge calculations

Our next results are concerned with investigating the accuracy of the different gauges, namely, the length and the

TABLE I. A comparison of the yields between results of Guan *et al.* (FE-DVR; prolate spheroidal coordinates) and the basis method (BS) and the RMT approach, both in spherical coordinates. The sine-squared pulse used has a photon energy of $\omega = 40$ eV and is 10 cycles in duration. The peak intensity, I_0, is varied from 10^{12} to 10^{15} W cm^{-2}. The percentage difference between the RMT method and the FE-DVR method is also listed, in parentheses.

I_0	FE-DVR	BS	RMT
10^{12}	2.330×10^{-6}	2.325×10^{-6}	2.325×10^{-6} (-0.22%)
10^{13}	2.330×10^{-5}	2.326×10^{-5}	2.325×10^{-5} (-0.22%)
10^{14}	2.327×10^{-4}	2.328×10^{-4}	2.328×10^{-4} ($+0.43\%$)
10^{15}	2.304×10^{-3}	2.352×10^{-3}	2.351×10^{-3} (-2.04%)

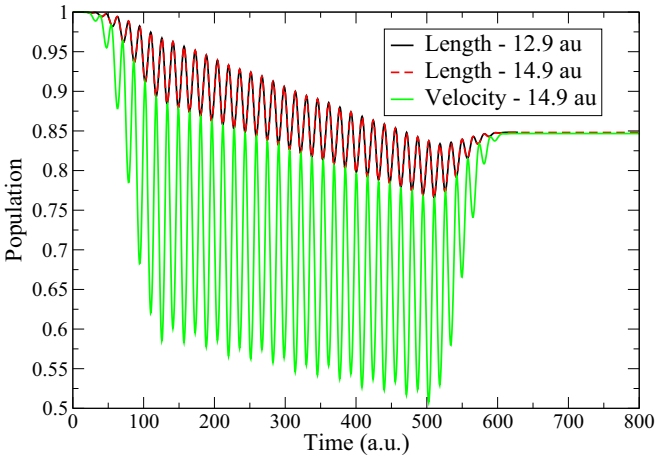

FIG. 5. (Color online) Comparison of the ground-state population as a function of time for H_2^+ in the length and velocity gauges for the pulse parameters given in [47]. Also shown are two inner-outer region boundary locations in the length gauge case; 12.9 and 14.9 a.u.

velocity gauges. For these calculations we compare results obtained by the pure basis (BS) and RMT methods.

In Fig. 5 we plot the ground-state population during the propagation. The population of field-free states is gauge dependent in the presence of an external EM field but gauge invariant when the vector potential returns to 0. Consistent with this fact we observe an agreement for the population corresponding to the different gauges, at times where $A(t)$ is equal to 0. For minima of the field the RMT length-gauge result agrees with the velocity-gauge calculation to a high degree.

In Fig. 6 we plot the calculated ionization yields for the various methods and gauges. We see that there is clear agreement for the final yield [as there should be, since $A(t) = 0$] and the yields during the pulse duration where $A(t)$ is equal to 0 except for the basis length-gauge calculations.

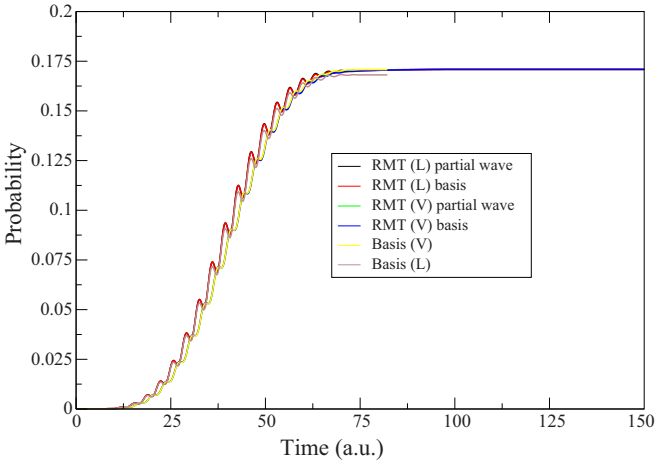

FIG. 6. (Color online) Yield for the basis and RMT methods in both the length (L) and the velocity (V) gauges. For the RMT method, "basis" or "partial wave" denotes the method used to calculate the yield.

IV. CONCLUSION

Since the development of the RMT method in 2008 [29], work has focused on various aspects of atomic systems [14,30,37]. In this paper, we have discussed the extension of the RMT approach to a molecular system. The work has focused on H_2^+ since it is the simplest molecular system. This extension reduces the dimensionality problems in H_2^+, since one can now have a full-basis inner region and have a finite-difference outer region which decouples the angular momenta terms as the hydrogenic approximation becomes valid [$V(r) \approx V_H(r)$]. The RMT method has been expanded to include the case where eigenstates contain a mixture l so that there is a transformation from an ungerade or gerade representation in the inner region to a representation consisting of a spherical-harmonic expansion. This work on H_2^+ has also been performed with the objective of approaching a treatment of H_2 which treats both electrons with a full correlation in the inner region but has one-electron outer-region trajectories. It is hoped that future work will expand on this existing formulation and code base and extend the RMT method to this new case.

ACKNOWLEDGMENTS

The authors would like to acknowledge the contributions of Prof. K. T. Taylor, Prof. P. Decleva, and Dr. Daniel Dundas during the preparation of this work. We are grateful to Prof. K. T. Taylor and Prof. P. Decleva for their constant interest and stimulating discussions. In addition, Prof. P. Decleva provided technical data used for comparisons during development and Dr. D. Dundas kindly ran calculations for comparison. During the preparation of this work support was provided by the FP7 Grant ERG-HPCAMO/256601 project and the COST Actions "XUV/X-Ray Light and Fast Ions for Ultrafast Chemistry" (CM1204) and "Advanced X-Ray Spatial and Temporal Metrology" (MP1203). C.Ó.B. acknowledges the Irish Centre for High-End Computing (ICHEC) for the use of computational resources under Project No. dcphy005c.

APPENDIX A: H_2^+ HAMILTONIAN AND DIPOLE OPERATOR BASIS REPRESENTATION IN A FINITE REGION

Our starting point is the evaluation of the eigenstates of the electronic Hamiltonian for the molecular hydrogen ion, $H\Phi_{n\lambda\mu}(\mathbf{r}) = \epsilon\Phi_{\epsilon\lambda\mu}(\mathbf{r})$, where ϵ is the eigenenergy value, λ the parity symmetry (gerade or ungerade), and μ the projection of the angular momentum along the internuclear axis. Assuming a coordinate system with the z axis along the internuclear axis and with the origin placed in the middle of the nuclei's distance, for the case of $\mu = 0$ states we can express the eigenstates on a spherical harmonic basis $Y_{lm_l}(\hat{r})$ as

$$\Phi_{\epsilon\lambda}(\mathbf{r}) = \sum_{l\in l_\lambda} \frac{1}{r} P_{\epsilon l}(r) Y_{l0}(\hat{r}). \tag{A1}$$

$\sum_{l\in l_\lambda}$ indicates the summation over members of the set l_λ, where the sets are defined as

$$l_\lambda = \begin{cases} \{0,2,4,\ldots,l_{\max}-2\} & \forall\ \lambda = 0, \\ \{1,3,5,\ldots,l_{\max}-1\} & \forall\ \lambda = 1. \end{cases}$$

The gerade-ungerade split of the angular momenta is imposed directly from analytic considerations of the molecular potential. Projection on the spherical harmonic basis provides the corresponding Schrödinger equation for the radial eigenfunctions $P_{nl}(r)$,

$$\left[h_l(r) + \sum_{l' \in l_\lambda} V_{l0,l'0}(r)\right] \frac{P_{\epsilon l'}(r)}{r} = \epsilon_{n\lambda} \frac{P_{\epsilon l}(r)}{r},$$

$$h_l(r) = -\frac{1}{2}\frac{\partial^2}{\partial r^2} + \frac{l(l+1)}{2r^2},$$

$$V_{l0,l'0}(r) = -2Z\sqrt{2l+1}\sqrt{2l'+1} \times \sum_L \frac{r_<^L}{r_>^{L+1}} \begin{pmatrix} l & L & l' \\ 0 & 0 & 0 \end{pmatrix}^2,$$

with $L = |l-l'|, |l-l'|+2, \ldots, l+l'$, and $l_> = \max(r, R_M/2)$, $l_< = \min(r, R_M/2)$, and the bracket-like symbol being the $3j$ symbol. For the $H_2{}^+$ case, the nuclear charge Z is set to 1.

In the general case, the eigenstates of the system are the bound and continuum. The continuum wave functions are not square integrable because they extend infinitely and do not asymptotically approach 0 with the distance from the nucleus. Rather they are asymptotically periodic. The first step in numerically calculating the eigenstates is to place them inside a spherical box of, say, radius, R_I [8,49,50]. This will discretize the full spectrum of the Hamiltonian (bound and continuum) and will make the continuum states square integrable. In this case, the eigenenergies can be characterized by a discrete index, as $\epsilon \to \epsilon_n \leftrightarrow n$, while their exact discretization will depend upon the λ symmetry.

Here, we choose to expand the radial functions $P_{nl}(r)$ in terms of a nonorthogonal, local, polynomial set, namely, the B-splines basis, $B_{ik}(r), i = 1, \ldots, N_s$, as [48,49]

$$P_{nl}(r) = \sum_i^{N_s} c_i^{(nl)} B_i(r). \tag{A2}$$

1. $H_2{}^+$ Hamiltonian

Following a standard procedure one can transform the TISE into a generalized eigensystem of the form

$$\sum_{l \in l_\lambda, l' \in l_\lambda} (\mathbf{H}_l + \mathbf{V}_{l',l})\mathbf{C}_l = \epsilon_{n\lambda} \sum_{l \in l_\lambda} \mathbf{S}\mathbf{C}_l, \tag{A3}$$

where $\mathbf{S}$ is the B-spline overlap matrix and the elements of the matrix are $S_{ij} = \int_r dr\, B_i B_j$, $\mathbf{H}_l$ is the B-spline overlap with the Hamiltonian,

$$H_l^{(ij)} = \frac{1}{2}\int_0^{R_I} dr \left[B_i' B_j' + l(l+1)\frac{B_i B_j}{r^2}\right], \tag{A4}$$

and the elements of the molecular potential matrix $\mathbf{V}_{l',l}$ given by $V_{l'l}^{(ij)} = \int_0^{R_I} dr\, B_i V_{l0,l'0}(r) B_j$.

Since the matrices required can be explicitly calculated, the only unknowns are the specific eigenenergies ($\epsilon_{n\lambda}$) and the associated B-spline coefficients $c_i^{(nl)}$, gathered in vector $\mathbf{C}_l$. Thus, provided the matrices are symmetric (or the Hamiltonian representation Hermitian) the system can be diagonalized to produce real-valued eigenenergies. This is certainly the case if we impose the extra (boundary) condition on the possible solutions $P_{nl}(R_I) = 0$ at both ends [within the B-splines basis this is easily done by excluding the first (B_1) and the last (B_{n_s}) B-splines from the set in Eq. (A2)]. In the present work this is not the proper way to ensure Hermiticity (or symmetricity of the associated matrices) of the operators. The reason for this is that we require solutions which are nonzero on the boundary surface, namely, solutions where $P_{nl}(R_I) \neq 0$, so as to ensure a nonzero probability current across the boundary surface. The alternative way of "Hermitizing" a non-Hermitian operator is by the addition of the so-called Bloch operator, being another central concept in the R-matrix theory. We relegate a more detailed discussion of this Bloch-operator method to the next section, to include any physical operator restricted in a finite region.

2. Dipole operators

The dipole operator for the length gauge is given by $D(\mathbf{r},t) = \mathbf{r}\cdot\mathbf{E}(t) = E(t) r\cos\theta$, while for the velocity gauge it is $\hat{D}(\mathbf{r},t) = \mathbf{p}\cdot\mathbf{A}(t)/c$. After use of Eq. (A1) the corresponding matrix element equations are written as

$$\hat{D}_{n\lambda,n'\lambda'}(t) = E(t)\langle n\lambda | r\cos\theta | n',\lambda'\rangle = E(t)\sum_{l\in l_\lambda}\sum_{l'\in l_{\lambda'}}\langle nl | r\cos\theta | n'l'\rangle$$

for the length-gauge dipole matrix elements, where use is made of the spherical harmonic expansion. For the velocity-gauge dipole matrix elements, the equivalent expression is

$$\hat{D}_{n\lambda,n'\lambda'}(t) = \langle n\lambda | \mathbf{p}\cdot\frac{\mathbf{A}(t)}{c} | n',\lambda'\rangle = \frac{A(t)}{c}\sum_{l\in l_\lambda}\sum_{l'\in l_{\lambda'}}\langle nl | -i\nabla\cdot\hat{z} | n'l'\rangle.$$

By the further use of the B-spline expansion of the radial solutions [Eq. (A2)] and some angular momentum algebra one has the main expression in terms of known quantities,

$$D_{n\lambda,n'\lambda'}(t) = \sum_{l\in l_\lambda, l'=l\pm1} \frac{l_>}{\sqrt{4l_>^2-1}} \mathcal{G}_{nl;n'l'}(t), \tag{A5}$$

with $l_> = \max(l,l')$ and where $\mathcal{G}$ is the respective matrix, $\mathcal{L}$ or $\mathcal{V}$,

$$\mathcal{L}_{nl;nl'}(t) = E(t)\int_0^{R_I} dr\, P_{nl}(r) r P_{n'l'}(r),$$

$$\mathcal{V}_{nl;nl'}(t) = \frac{A(t)}{c}\int_0^{R_I} dr\, P_{nl}(r)\left[\frac{d}{dr} + (l-l')\frac{l_>}{r}\right] P_{n'l'}(r),$$

where the specific choice depends on the gauge: length and velocity, respectively. Thus, this can be calculated explicitly following diagonalization of Eq. (A3).

The dipole terms for the outer region from Eq. (11), $\langle l0|D(\mathbf{r},t)|l'0\rangle$, are the standard length- and velocity-gauge terms for partial waves (see [29]).

APPENDIX B: RESTORING THE HERMITICITY OF THE FIELD-FREE HAMILTONIAN OPERATOR IN A RESTRICTED SPATIAL REGION USING THE BLOCH OPERATOR

Now we describe how the Bloch operator [51] is used to make the Hamiltonian Hermitian in the inner region $0 \leqslant r \leqslant R_{\rm I}$, where the space of wave functions has arbitrary boundary conditions of the form $\alpha\Phi(\mathbf{R}_{\rm I}) + \beta\Phi(\mathbf{R}_{\rm I}) = 0$. The Laplacian operator will be Hermitian if [52]

$$\langle\Phi'|H|\Phi\rangle - \langle\Phi'|H|\Phi\rangle^{\star} = 0, \tag{B1}$$

because the definition of a Hermitian operator is such that its matrix elements are equal to their own conjugate transpose.

This condition holds for all Hamiltonian terms that do not contain derivatives in the inner region. Applying Eq. (B1), the kinetic operator $T = -\nabla^2/2$ term of the field-free part of the Hamiltonian and the dipole interaction term in the velocity gauge $D(\mathbf{r},t) = \frac{\mathbf{A}(t)}{c}\cdot(-i\nabla)$ will be non-Hermitian operators. Both operators are now considered one at a time.

1. Kinetic operator *T*

Substitution of Eq. (A1) in formula (B1) followed by standard differential calculus manipulations results in

$$\langle n\lambda|T|n'\lambda'\rangle - \langle n'\lambda'|T|n\lambda\rangle = -\frac{1}{2}\sum_{l\in l_\lambda, l'\in l_{\lambda'}}\left[P_{nl}(R_{\rm I})\frac{d}{dr}P_{n'l'}(R_{\rm I}) - P_{n'l'}(R_{\rm I})\frac{d}{dr}P_{nl}(R_{\rm I})\right], \tag{B2}$$

where in order to ensure continuity at the center of symmetry the value $P_{nl}(0) = 0$ is used [48], while $P_{nl}(r)$ can take arbitrary values and arbitrary derivatives at the boundary. At this stage we introduce the Bloch operator, which is generally defined as [21]

$$\hat{L}_h = \frac{1}{2}\delta(r - R_{\rm I})\left(\frac{d}{dr} - \frac{\alpha - 1}{r}\right), \tag{B3}$$

where α is a constant which can be chosen without constraints. As shown below, the following considerations are not affected by the particular choice of α. In our calculations we have set $\alpha = 0$. For the Bloch operator $\hat{L}_h$ the following relation holds:

$$\langle n\lambda|\hat{L}_h|n'\lambda'\rangle - \langle n'\lambda'|\hat{L}_h|n\lambda\rangle = \frac{1}{2}\sum_{l\in l_\lambda, l'\in l_{\lambda'}}\left[P_{nl}(R_{\rm I})\frac{d}{dr}P_{n'l'}(R_{\rm I}) - P_{n'l'}(R_{\rm I})\frac{d}{dr}P_{nl}(R_{\rm I})\right]. \tag{B4}$$

Now by modifying the kinetic operator as $\hat{T} = T + \hat{L}_h$ and considering Eqs. (B2) and (B4), we find that

$$\langle n\lambda|\hat{T}|n'\lambda'\rangle - \langle n'\lambda'|\hat{T}|n\lambda\rangle = 0. \tag{B5}$$

Therefore, the matrix representation of the kinetic operator in the inner region, augmented by the above Bloch operator, is Hermitian, and as such its diagonalization will provide real eigenvalues.

2. Dipole interaction term in the velocity gauge

Following similar considerations as in the case of the kinetic operator we arrive at the result that a Hermitian velocity-gauge interaction operator can be obtained as $\hat{D} = D + L_d$, where L_d is

$$L_d = -i\frac{1}{2}\frac{A(t)}{c}\delta(r - R_{\rm I})\cos\theta. \tag{B6}$$

APPENDIX C: RECURSIVE COMPUTATION OF THE HIGHER DERIVATIVES IN THE INNER-REGION TDSE

Propagation of the inner-region TDSE Eq. (10a) through an explicit pth-order propagator (e.g., the Taylor propagator) requires the repeated multiplication of the wave function by the Hamiltonian; $\hat{H}^p\Phi(t)$. This operation, in turn, requires one to calculate the pth-order time derivative of the boundary surface term. Below we give in more detail the relevant formulas for this calculation.

We start by noting that the second derivative of the coefficients is given by the equation

$$\frac{d^2}{dt^2}C_{n\lambda}(t) = -i\sum_{n'\lambda'}H_{n\lambda,n'\lambda'}(t)\frac{d}{dt}C_{n'\lambda'}(t) + i\sum_{l\in l_\lambda}P_{nl}(R_{\rm I})\frac{d}{dt}F_l(r,t).$$

The pth derivative is

$$\frac{d^p}{dt^p}C_{n\lambda}(t) = -i\sum_{n'\lambda'}H_{n\lambda,n'\lambda'}(t)\frac{d^{p-1}}{dt^{p-1}}C_{n'\lambda'}(t) + i\sum_{l\in l_\lambda}P_{nl}(R_{\rm I})\frac{d^{p-1}}{dt^{p-1}}F_l(r,t).$$

Analogous to the hydrogen case, from Eq. (7) the higher derivatives for the Taylor expansion on a grid $r_j, j = 1,2,\ldots$ are given by

$$f_l^{(p)}(r_j,t) = -i\frac{dt}{p}\sum_{l'}H_{l,l'}(r_j,t)f_{l'}^{(p-1)}(r_j,t) \tag{C1}$$

and

$$C_{n\lambda}^{(p)}(t) = \frac{-i\,dt}{p}\sum_{n'\lambda'}H_{n\lambda,n'\lambda'}(t)C_{n'\lambda'}^{(p-1)}(t) + \frac{i\,dt}{p}\sum_{l\in l_\lambda}P_{nl}(R_{\rm I})F_l^{(p-1)}(r,t),$$

where the partial-wave terms for the inner boundary are recalculated as

$$f_{l_\lambda}^{(p)}(r_j,t) = \sum_n C_{n\lambda}^{(p)}(t)P_{nl_\lambda}(r_j) \quad \forall\ r_j \leqslant R_{\rm I}. \tag{C2}$$

The Taylor sums are then

$$f_l(r_j,t+\tau) = \sum_p^P f_l^{(p)}(r_j,t) \quad \forall j \geqslant b, \tag{C3}$$

$$C_{n\lambda}(t+\tau) = \sum_p^P C_{n\lambda}^{(p)}(t). \tag{C4}$$

[1] B. Wolter, M. G. Pullen, M. Baudisch, M. Sclafani, M. Hemmer, A. Senftleben, C. D. Schröter, J. Ullrich, R. Moshammer, and J. Biegert, Phys. Rev. X **5**, 021034 (2015).

[2] P. Tzallas, E. Skantzakis, L. A. A. Nikolopoulos, G. D. Tsakiris, and D. Charalambidis, Nat. Phys. **7**, 781 (2011).

[3] E. Cormier and P. Lambropoulos, J. Phys. B: At. Mol. Opt. Phys. **30**, 77 (1997).

[4] H. M. Tetchou Nganso, Yu. V. Popov, B. Piraux, J. Madroñero, and M. G. Kwato Njock, Phys. Rev. A **83**, 013401 (2011).

[5] T. K. Kjeldsen, L. B. Madsen, and J. P. Hansen, Phys. Rev. A **74**, 035402 (2006).

[6] G. L. Kamta and A. D. Bandrauk, Phys. Rev. A **71**, 053407 (2005).

[7] A. Palacios, S. Barmaki, H. Bachau, and F. Martín, Phys. Rev. A **71**, 063405 (2005).

[8] M. Awasthi, Y. V. Vanne, and A. Saenz, J. Phys. B **38**, 3973 (2005).

[9] J. Caillat, J. Zanghellini, M. Kitzler, O. Koch, W. Kreuzer, and A. Scrinzi, Phys. Rev. A **71**, 012712 (2005).

[10] L. A. A. Nikolopoulos and P. Lambropoulos, J. Phys. B **39**, 883 (2006).

[11] A. D. Bandrauk, S. Chelkowski, D. J. Diestler, J. Manz, and K.-J. J. Yuan, Phys. Rev. A **79**, 023403 (2009).

[12] X. Guan, O. Zatsarinny, K. Bartschat, B. I. Schneider, J. Feist, and C. J. Noble, Phys. Rev. A **76**, 053411 (2007).

[13] X. Guan, E. B. Secor, K. Bartschat, and B. I. Schneider, Phys. Rev. A **84**, 033420 (2011).

[14] L. R. Moore, M. A. Lysaght, L. A. A. Nikolopoulos, J. S. Parker, H. W. van der Hart, and K. T. Taylor, J. Mod. Opt. **58**, 1132 (2011).

[15] D. Dundas, J. Chem. Phys. **136**, 194303 (2012).

[16] T. Carette, J. M. Dahlström, L. Argenti, and E. Lindroth, Phys. Rev. A **87**, 023420 (2013).

[17] J. Feist, O. Zatsarinny, S. Nagele, R. Pazourek, J. Burgdörfer, X. Guan, K. Bartschat, and B. I. Schneider, Phys. Rev. A **89**, 033417 (2014).

[18] F. Catoire, R. E. F. Silva, P. Rivière, H. Bachau, and F. Martín, Phys. Rev. A **89**, 023415 (2014).

[19] H. G. Muller, Phys. Rev. A **60**, 1341 (1999).

[20] M. Awasthi, Y. V. Vanne, A. Saenz, A. Castro, and P. Decleva, Phys. Rev. A **77**, 063403 (2008).

[21] P. G. Burke, A. Hibbert, and W. D. Robb, J. Phys. B **4**, 153 (1971).

[22] P. G. Burke, *R-Matrix Theory of Atomic Collisions (Springer Ser. At. Opt. Plasma Phys.)* (Springer, Berlin, 2011), p. 745.

[23] D. Madden, J. Tennyson, and R. Zhang, J. Phys. Conf. Ser. **300**, 012017 (2011).

[24] P. G. Burke and W. D. Robb, Adv. At. Mol. Phys. **11**, 143 (1976).

[25] P. G. Burke and K. T. Taylor, J. Phys. B **8**, 2620 (1975).

[26] P. G. Burke and V. M. Burke, J. Phys. B **30**, L383 (1997).

[27] H. W. van der Hart, M. A. Lysaght, and P. G. Burke, Phys. Rev. A **76**, 043405 (2007).

[28] X. Guan, C. J. Noble, O. Zatsarinny, K. Bartschat, and B. I. Schneider, Phys. Rev. A **78**, 053402 (2008).

[29] L. A. A. Nikolopoulos, J. S. Parker, and K. T. Taylor, Phys. Rev. A **78**, 063420 (2008).

[30] M. A. Lysaght, L. R. Moore, L. A. A. Nikolopoulos, J. S. Parker, H. W. Hart, and K. T. Taylor, in *Quantum Dynamic Imaging*, *CRM Series in Mathematical Physics*, edited by A. D. Bandrauk and M. Ivanov (Springer, New York, 2011), pp. 107–134.

[31] P. G. Burke, P. Francken, and C. J. Joachain, J. Phys. B **24**, 751 (1991).

[32] M. A. Lysaght, P. G. Burke, and H. W. van der Hart, Phys. Rev. Lett. **101**, 253001 (2008).

[33] S. Hutchinson, M. A. Lysaght, and H. W. van der Hart, Phys. Rev. A **88**, 023424 (2013).

[34] K. A. Berrington, W. B. Eissner, and P. H. Norrington, Comput. Phys. Commun. **92**, 290 (1995).

[35] O. Zatsarinny, Comput. Phys. Commun. **174**, 273 (2006).

[36] E. S. Smyth, J. S. Parker, and K. T. Taylor, Comput. Phys. Comm. **114**, 1 (1998).

[37] J. Wragg, J. S. Parker, and H. W. van der Hart, Phys. Rev. A **92**, 022504 (2015).

[38] L. Tao and A. Scrinzi, New J. Phys. **14**, 013021 (2012).

[39] A. Scrinzi, New J. Phys. **14**, 085008 (2012).

[40] L. Torlina and O. Smirnova, Phys. Rev. A **86**, 043408 (2012).

[41] L. Torlina, M. Ivanov, Z. B. Walters, and O. Smirnova, Phys. Rev. A **86**, 043409 (2012).

[42] L. Torlina, F. Morales, H. Muller, and O. Smirnova, J. Phys. B **47**, 204021 (2014).

[43] E. Cormier and P. Lambropoulos, J. Phys. B **77**, 1667 (1996).

[44] C. Ó Broin and L. A. A. Nikolopoulos, Comput. Phys. Commun. **183**, 2071 (2012).

[45] C. Ó Broin and L. A. A. Nikolopoulos, Comput. Phys. Commun. **185**, 1791 (2014).

[46] B. H. Bransden and C. J. Joachain, *Physics of Atoms and Molecules* (Pearson Education, India, Delhi, 2003).

[47] D. Dundas, J. F. McCann, J. S. Parker, and K. T. Taylor, J. Phys. B **33**, 3261 (2000).

[48] F. Martín, J. Phys. B **32**, R197 (1999).

[49] H. Bachau, E. Cormier, P. Decleva, J. E. Hansen, and F. Martín, Rep. Prog. Phys. **64**, 1815 (2001).

[50] S. Barmaki, S. Laulan, H. Bachau, and M. Ghalim, J. Phys. B **36**, 817 (2003).

[51] C. Bloch, Nucl. Phys. **4**, 503 (1957).

[52] C. Cohen-Tannoudji, B. Diu, and F. Laloë, *Quantum Mechanics, Vol. 1* (Wiley-VCH Verlag, Weinheim, Germany, 1977), p. 914.